

Spatial decorrelation in broad-area edge-emitting semiconductor amplifiers

S. Barland¹, X. Hachair¹, M. Giudici^{1,a}, S. Balle^{1,b}, J.R. Tredicce¹, G. Tissoni², L. Spinelli²,
L. Lugiato², and M. Brambilla³

¹ Institut Non-linéaire de Nice, UMR 6618 CNRS, Université de Nice Sophia-Antipolis, 06560 Valbonne, France

² INFN, Dipartimento di Scienze, Università dell'Insubria, Via Valleggio 11, 22100 Como, Italy

³ INFN, Dipartimento di Fisica Interateneo, Università e Politecnico di Bari, Via Orabona 4, 70126 Bari, Italy

Received 29 June 2004

Published online 26 October 2004 – © EDP Sciences, Società Italiana di Fisica, Springer-Verlag 2004

Abstract. We analyze experimentally the spatio-temporal dynamics of the transverse structures appearing in broad area edge-emitting semiconductor amplifiers under CW optical injection. We demonstrate that, in certain conditions, the light reflected by the system exhibits a multi-peaked structure whose dependence on the parameters suggests an interpretation in terms of cavity solitons. These structures can exhibit self-pulsations with periods of the order of few milliseconds, which we explain in terms of regenerative thermal oscillations. In a particular device, we generate two single-peak structures which are spatially uncorrelated, as required for cavity solitons. A microscopic model shows good agreement with the main body of the experimental results.

PACS. 42.70.Nq Other nonlinear optical materials; photorefractive and semiconductor materials – 42.65.Tg Optical solitons; nonlinear guided waves

1 Introduction

Applications to information technology are one of the goals of the extensive work in the field of transverse patterns formation in nonlinear optical systems [1–6]. The problem of the correlation among different parts of an optical pattern can be solved by generating spatial structures which are localized in a portion of the transverse plane in such a way that they are individually addressable and independent of one another. Such structures, called cavity solitons (CS) have been theoretically predicted in nonlinear materials inside a cavity [7–14]. These phenomena have been observed in macroscopic cavities [15–17] and in systems with feedback [18–20].

Most interesting from the practical viewpoint is the case in which the medium is a semiconductor. In fact, we consider an optical cavity containing a semiconductor medium and driven by a stationary holding-beam as it was theoretically described in [21]. Generation of 2D spatial patterns and phenomena of light localization have been observed [22]; a clear-cut experimental demonstration of CS in semiconductor devices has been obtained recently [23], using a 2D device (VCSEL below threshold)

with a large Fresnel number, only after overriding a number of limiting factors linked to the thermal heating of the sample, and to its homogeneity in the transverse plane.

In this joint experimental-theoretical investigation we focus on active broad-area devices with 1D geometry. We show the formation of isolated intensity peaks, that can be spontaneously generated by the system or induced by the injection of pulses in the transverse section; in the latter case, they persist after the passage of the pulse. Upon variation of the wavelength of the driving field, we obtain first a one-peaked structure which is a cavity soliton candidate. By increasing gradually the modulus of the (negative) cavity detuning, the one-peaked structure evolves to multi-peaked structures with three and five spatially correlated peaks. Our numerical simulations, which agree very well with the experimental findings, show that these structures are portions of a periodic 1D pattern of the kind first predicted in the framework of the paradigmatic model [24], and that the finite size of the sample allows for accommodating only a limited odd number of peaks of the pattern according to the value of the cavity detuning.

Finally, under appropriate conditions we obtain emission on two peaks which are shown to be dynamically independent of each other, thus proving that the correlation length of these structures is actually shorter than the transverse size of the device. This provides us with one of the necessary conditions for the formation of cavity

^a e-mail: massimo.giudici@inln.cnrs.fr

^b Also at Institut Mediterrani d'Estudis Avançats, IMEDEA (CSIC–Universitat de les Illes Balears), C/Miquel Marquès 21, 07190 Esporles, Spain.

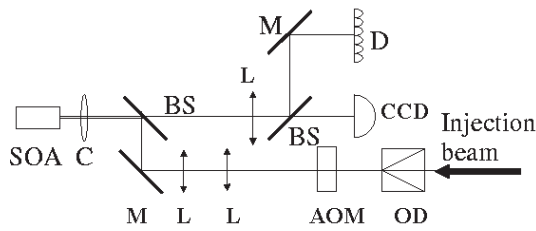


Fig. 1. Scheme of the experimental set-up. SOA: broad-area semiconductor amplifier, C: collimator, BS: beam splitter, L: lenses, M: mirror, AOM: acousto-optic modulator, OD: optical diode, CCD: CCD camera, D: linear array of detectors.

solitons. However, a full validation of these two peaks in terms of CS is still missing due to thermal effects and possibly inhomogeneities in the semiconductor medium, but we indicate possible routes to overcoming the present limits.

2 The experiment

The experimental set-up is shown in Figure 1. The semiconductor amplifier is a commercial 980 nm edge-emitting laser (Thorlabs L9801E3P1) having a transverse section of $100 \mu\text{m} \times 1 \mu\text{m}$. The front facet is antireflection coated. Longitudinal modes are separated by 39 GHz from which we infer a longitudinal length of the laser cavity of the order of 1 mm (index of refraction of 3.5). The laser is mounted on a thermally stabilized submount (better than $0.01 \text{ }^\circ\text{C}$) and it is biased by a very stable (better than 0.01 mA) current source. Since we operate the laser as an optical amplifier we keep the bias current (I) above transparency and below threshold. In order to reduce the divergence of the laser output we use a high numerical aperture (0.68) collimator. The near field emission of the amplifier is obtained by using crossed mounted cylindrical lenses and recorded on a CCD camera. We also use a 16-element linear silicon PIN photodiode array (100 kHz bandwidth) in order to monitor the intensity output from small regions of the transverse plane. This is useful for detecting synchronously the time behavior of coexisting localized structures.

The holding-beam is provided by a tunable, thermally-stabilized, high-power semiconductor laser (master laser) emitting around $\lambda \sim 980 \text{ nm}$. The maximum power available for injection is around 8 mW. An optical isolator ($>30 \text{ dB}$ isolation) avoids back reflections from the amplifier and from the detection system onto the master laser. The optical power injected into the amplifier is controlled by an acousto-optic modulator (AOM), and the holding-beam is aligned with the amplifier's optical axis and expanded to guarantee a homogeneous intensity profile over the whole transverse section of the amplifier. During our experiment we varied two main parameters: the optical injection power P and the detuning $\delta\nu = \nu_c - \nu_0$ between the master laser emission frequency (ν_0) and the closest longitudinal cavity resonance of the amplifier (ν_c). Consequently, the detuning range is limited by the separation

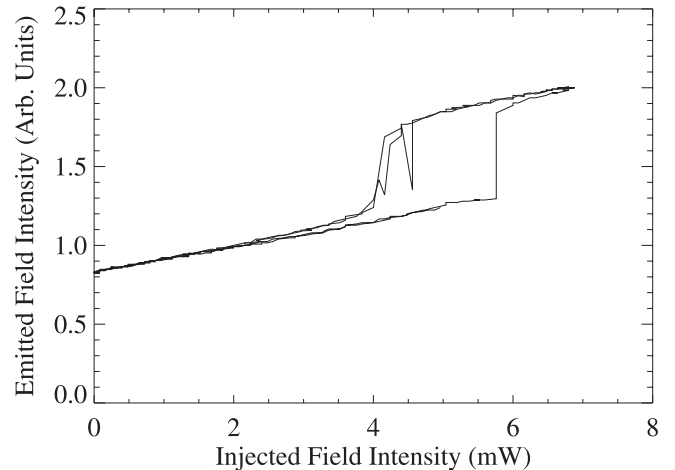


Fig. 2. Total output from the amplifier as the injected power is varied, we observe hysteresis in the amplifier response. Pumping current of the amplifier: $I = 0.98I_{th}$.

between two consecutive longitudinal modes of the amplifier ($0 < \delta\nu < 39 \text{ GHz}$).

One of the main features of cavity solitons is that they may exist in parameter regions such that an optical pattern coexists with a homogeneous state of low intensity. Thus we modulate the injected power with the AOM and we look for hysteretical behavior of the total output power as a function of the injection power. We observed that the most favorable conditions correspond to injection frequencies close to the amplifier cavity resonances that lie in the vicinity of the amplifier gain peak. Figure 2 shows a typical trace obtained in such a case, and by looking at the CCD camera we can determine that the low intensity branch corresponds to homogeneous emission while the high intensity branch corresponds to a single-peak structure (Fig. 3). Since for the biasing current used in the experiment ($0.80I_{th} < I < 0.99I_{th}$) the gain curve of the amplifier is broader than 1.5 THz, there is a large range of master laser frequency for which the interaction with the amplifier gives rise to hysteretical switching between the homogeneous state and a patterned emission. Indeed, a variation of the frequency of the master laser by multiples of 39 GHz allows to reproduce the observed behavior, thus evidencing the role of the amplifier cavity resonances. We must finally note that the width of the hysteresis cycle depends on the frequency of the modulating signal applied to the AOM; in addition, for low modulation frequency, it is observed that the hysteresis cycle is described in the reverse direction, as previously described in the literature [25]. As we discuss later on, we explain these facts by a thermal drift of the amplifier's resonances due to the strong changes in intracavity field that cannot be compensated by the thermal stabilization system.

By fine-tuning the wavelength of the injected field around any of the cavity resonances of the amplifier that lie close to the gain peak, the spatial profile of the emission changes. We fix the injected optical power to the value corresponding to the center of the hysteresis cycle (Fig. 2), and as the injection frequency is changed, we observe that

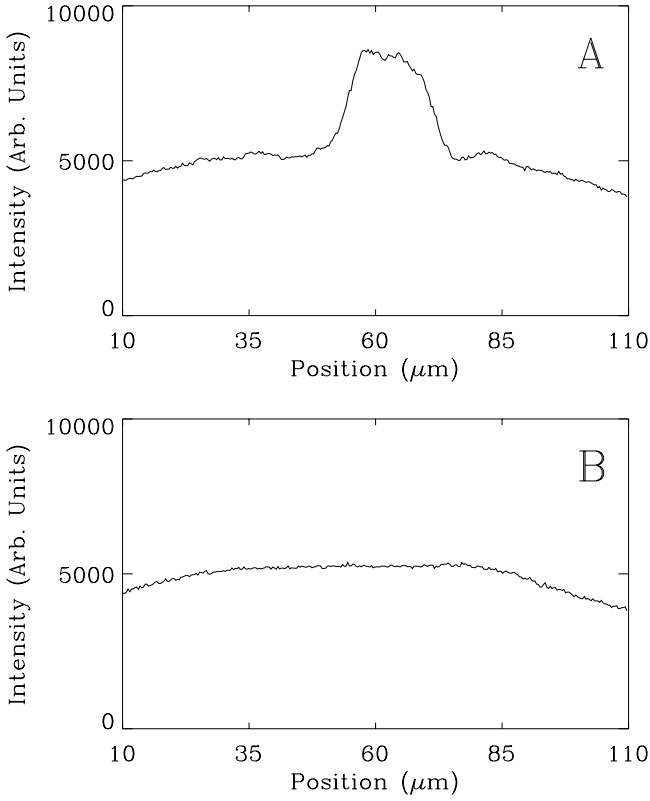


Fig. 3. Spatial profile (near-field) of the amplifier emission corresponding to the upper branch of the bistability cycle (A) and to the lower branch of the bistability cycle (B). The parameters are the same of Figure 2.

the spatial pattern corresponding to the high intensity branch evolves from a single-peak into more complicated structures with three and finally five peaks as we increase the detuning (see Figs. 4 and 5). It is important noting that the profiles shown in Figure 5 cannot be interpreted as Hermite-Gauss modes of a rectangular cavity. Hermite-Gauss modes presents a multi-peak structure but the amplitude of the peaks grows when approaching the borders of the structure. Instead, in our case, we observe that the amplitude of the peaks decreases from the center of the structure, as observed for filamentation [26].

In order to clarify the possibility for these structures to be cavity solitons, we have performed different tests. The most important is related to the use of a writing beam: a small ($\sim 10 \mu\text{m}$ waist) beam superimposed to the holding-beam and coherent with it. The writing beam targets a point of the transverse plane of the amplifier in order to switch-on the localized structure from the homogeneous emission state where the system is prepared by proper setting of the holding-beam intensity. This test has revealed that (i) it is possible to create a single-peak structure in a relatively wide region of parameter space, (ii) it is not possible to create the single-peak structure in another point than the one where it switches on spontaneously for high enough power of the holding-beam, (iii) the peaks of the structures in Figures 5b and 5c cannot be switched on independently. This last observation indicates that the

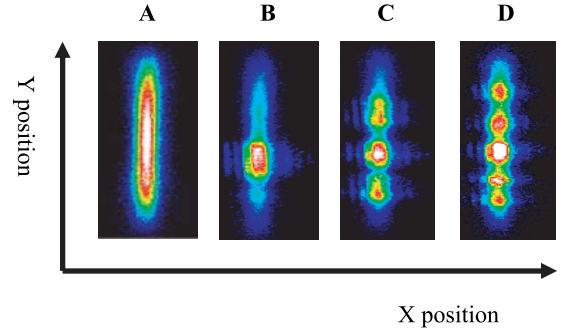


Fig. 4. Two-dimensional profiles of the amplifier emission (near-field) as the frequency of the injected field is increased around a resonance of the amplifier cavity. Since it is impossible to measure the real detuning between the injected field and the cavity resonance, we assume that $\Delta\nu = 0$ GHz for the situation where a single-peak profile is observed. (a) $\Delta\nu = 6$ GHz, (b) $\Delta\nu = 0$ GHz, (c) $\Delta\nu = -3.5$ GHz, (d) $\Delta\nu = -6.5$ GHz. The parameter values correspond to the center of the hysteresis cycle of Figure 2: $P = 6$ mW, $I = 0.98I_{th}$. The intensity level is represented by a color scale from black to white.

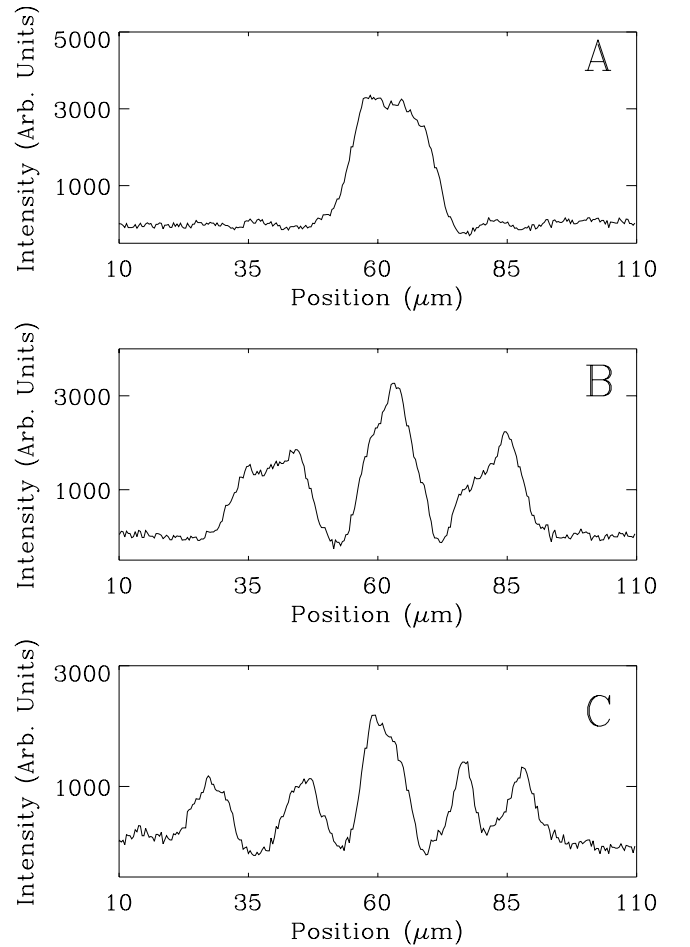


Fig. 5. One-dimensional profiles corresponding to the profiles of Figure 4 with subtraction of the background emission (no injection); A: $\Delta\nu = 0$ GHz, B: $\Delta\nu = -3.5$ GHz, C: $\Delta\nu = -6.5$ GHz. $P = 6$ mW, $I = 0.98I_{th}$.

observed structure cannot be considered an ensemble of independent entities. As a second test, we tried to use a phase gradient in order to move the single-peak structure, as predicted for cavity solitons, but the bright spot remains always pinned at the same point.

More insights can be obtained by monitoring the time behavior of these structures by a fast photo-detector (100 kHz bandwidth), instead of the time-averaging CCD camera. This test reveals that the structures observed in Figure 5 exhibit periodic pulsing from the on-state to the off-state on a timescale of few milliseconds, characteristic of thermal drifts in the cavity resonances [25] (this behavior can be seen in Fig. 7, panel 5, discussed further in this article). The application of the writing beam, targeting the single-peak structure, affects the flickering period and it can even stabilize the structure in the on-state, but as soon as it is removed, the oscillation restarts. In addition, we have observed that the flickering period can also be controlled by changing the phase of the writing beam with respect the phase of the holding-beam: for a relative phase difference of π , the flickering frequency is minimal and the structure stays most of the time in the off-state. Removing the writing beam, the flickering frequency comes back to the value previous to the application of the writing beam. These observations indicate that the structure is oscillating with a period imposed by the local value of the injected field, as already reported in [25]. The self-oscillating character of the structures prevents from full controlling their on/off state by mean of the writing-beam. A full experimental assessment of the single-peak structure in terms of cavity soliton, as the one performed in [23], requires to get rid of the thermal drift. This may be achieved using devices with a better heat sinking and further tests are in progress in this direction.

In general, we are not able to switch more than one single-peak structure in the transverse plane of the amplifier. In fact, considering that the size of the single-peak structure is approximately $25 \mu\text{m}$ and that the length scale of the boundary layers is of this same order of magnitude, there is not enough “room” to write a second independent single-peak structure. Moreover, the single-peak structure appears always pinned at the same central point of the transverse plane. This localization could be induced by some current or thermal gradient in the amplifier section or by some material defect in the laser facets, so we tried several nominally identical amplifiers in order to assess the influence of these device-dependent characteristics. We found the same qualitative behavior but, interestingly, every amplifier had different pinning positions for the single-peak structure. This pinning effect has recently been attributed (in the case of vertical cavity amplifiers) to inhomogeneities in the semiconductor layers, introduced during the fabrication process [23].

In a particular device, pinning occurred at the sides of the transverse section of the amplifier, leaving enough room for placing a second single-peak structure. In this device it has been possible to switch two single-peak structures close to the borders of the transverse section (see Fig. 6).

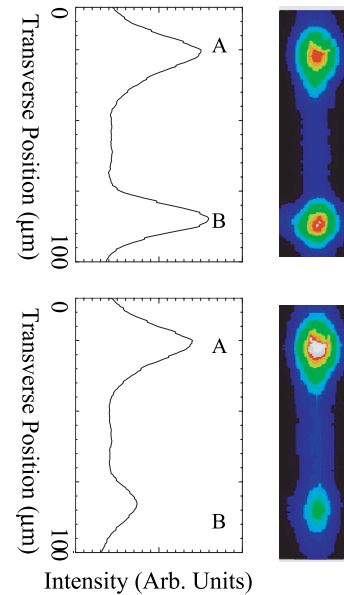


Fig. 6. Time-averaged near-field profile of the amplifier emission (right) and respective vertical cross-section (left) for the device where the two single-peak structures are pinned at the borders. The intensity level is represented by a color scale from black to white. Upper panel: $I = 0.995I_{th}$ mA, $P = 8$ mW: both structures are in the high-power state, lower panel: $I = 0.995I_{th}$ mA, $P = 6$ mW, the structure *A* is in the high-power state while the structure *B* is flickering resulting in a lower averaged emission level (see Fig. 7, panel 5).

In Figure 6 we show the time-averaged emission profile of the amplifier for two different holding power levels and for $I = 0.995I_{th}$. In the upper panel, corresponding to holding-beam power $P = 8$ mW, both structures are switched on and they have approximately the same (averaged) intensity. As the injected power is decreased to $P = 6$ mW (lower panel in Fig. 6) the time-averaged profile shows that the structure *B* is in a low-power state while the structure *A* remains on the high-power state.

A more complete information is obtained by examining the time behavior of each of these single-peak structures, which can be obtained by picking the signal from the elements of the linear detector array that are detecting these structures. In Figure 7 we show the dependence of the dynamics of each structure as the power in the holding-beam is varied. The upper (lower) trace corresponds to the single-peak structure called *A* (*B*) in Figure 6, and they have been shifted for the sake of clarity. For $I = 0.980I_{th}$ and low power in the holding-beam ($P = 5$ mW, see Fig. 7-1), structure *B* is constantly in the low-power state, while structure *A* is most of the time in the low-power state but sporadically it exhibits pulses towards the high-power state. These pulses have an almost constant duration and amplitude, but the time-interval between pulses is changing randomly (see [25]). Increasing the holding-beam power ($P = 6$ mW, Fig. 7-2), the switching rate of structure *A* to its the high-power state increases until, for $P = 7$ mW (Fig. 7-3), structure *A* remains now most of the time in the high-power state, while structure *B* keeps

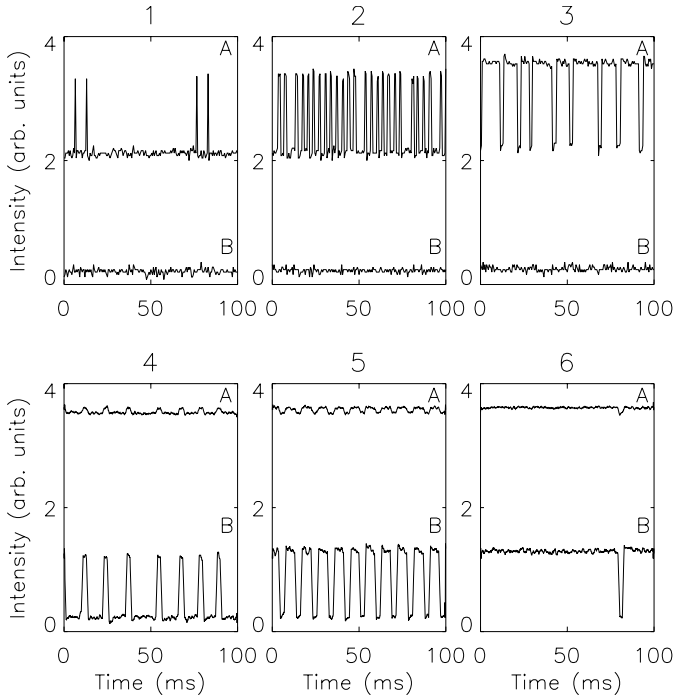


Fig. 7. Temporal evolution of the intensity of each of the two single-peak structures shown in Figure 6 as the injection power is increased. The time trace of structure 6 A has been shifted of 2 vertical units for clarity. (1) $P = 5$ mW, $I = 0.98I_{th}$ mA, (2) $P = 6$ mW, $I = 0.98I_{th}$, (3) $P = 7$ mW, $I = 0.98I_{th}$, (4) $P = 5$ mW, $I = 0.995I_{th}$, (5) $P = 6$ mW, $I = 0.995I_{th}$, (see corresponding time-integrated profile in Figure 6, lower panel). (6) $P = 7$ mW $I = 0.995I_{th}$. Finally (not shown), for $P = 8$ mW, both structures are constantly on (see 6, upper panel).

staying constantly in the low-power state. Further increasing of the holding-beam power to the maximum level available in our set-up ($P = 8$ mW), leads to a situation where structure A is switching to the low-state only sporadically, while structure B remains in the low-power state. In order to bring the structure B to the high-power state it is necessary to increase slightly the amplifier pumping current. In Figure 7-4, $I = 0.995I_{th}$ and $P = 5$ mW: structure A is now constantly in the on-state, but structure B is switching to the high-power state. Increasing the holding-beam power to $P = 6$ mW (Fig. 7-5) makes structure B to periodically switch from the high-power state to the low-power state, while structure A remains in the on-state and finally, for $P = 7$ mW (Fig. 7-6) both structures are almost constantly in the on-state.

This test proves that (i) the two structures are not correlated and one can flicker while the other keeps constantly in the same state and (ii) for the maximum holding-beam power available in our set-up ($P = 8$ mW), the activation of one structure requires a pumping current value of the amplifier slightly larger than for the activation of the second one. This difference is probably due to inhomogeneities of parameters along the device, e.g., the current profile or the heat extraction.

The sequence observed for each single-peak structure may be explained in term of self-regenerative thermal oscillations [25]. As the structures switch on, the changes in intracavity field induce a slow change in the temperature of the active region that shifts the cavity resonances until the structure is not stable anymore. At this point, the structure switches off and the emission level drops suddenly. The local temperature then recovers slowly and, after a while, the condition for stability of the structures is restored and the structures switch on again restarting the cycle. If the injection power is far above (far below) the switching point the temperature variation is not strong enough to affect the stability (the instability) of the structure and therefore this remains constantly on (off). This hypothesis explains the existence of two well separate time scales in the time series, justifies the extremely low time scale of the fluctuations and explains why for large injection power the structure is most of the time on while for low injection power it is most time off. It has been theoretically predicted that thermal effects leading to thermal drift of cavity resonance may induce these self-regenerative oscillations [27].

3 Theoretical model and comparison with experiments

We consider a model describing a laser diode with a large transverse section, in which the active material consists of few Quantum Wells of GaAs/AlGaAs type (MQW). Current is injected into the sample to create a population inversion, but the device is kept below the laser threshold.

The basic equations governing the dynamics of the system are derived in the paraxial and slowly varying envelope approximations, mean field limit and single longitudinal mode approximation [28, 29].

The geometry of the device makes the system essentially 1-dimensional: the dynamical equations can be therefore cast in the following form

$$\frac{\partial \tilde{E}}{\partial t} = -(1 + i\theta)\tilde{E} + \tilde{E}_I + i\Sigma\chi_{nl}\tilde{E} + i\frac{\partial \tilde{E}}{\partial x^2} \quad (1)$$

$$\frac{\partial \tilde{N}}{\partial t} = -\gamma \left[\tilde{N} - \tilde{I} - \Im m(\chi_{nl})|\tilde{E}|^2 - d\frac{\partial \tilde{N}}{\partial x^2} \right]. \quad (2)$$

The dynamical variables are the adimensional electric field

$$\tilde{E} = \sqrt{\frac{\epsilon_0\tau_r L_A}{\hbar N_0}} E, \quad (3)$$

and the normalized carrier density $\tilde{N} = N/N_0$, where ϵ_0 is the vacuum dielectric constant, τ_r is the nonradiative recombination rate of carriers, L_A is the thickness of the active material, and N_0 is the carrier density at transparency.

\tilde{E}_I is the adimensional slowly varying envelope of the field injected into the cavity, at frequency ω_0 , propagating through the material with velocity $v = c/n_b$, where n_b is

the background refractive index of the semiconductor. \tilde{I} is the normalized injected current.

Time is scaled to the photon lifetime $\tau_{ph} = 2L/vT$, with L being the cavity length and T the mean value of the front (T_F) and back (T_B) mirror transmissivity, while the transverse coordinate x is scaled to the diffraction length $l_a = \sqrt{\tau_{ph}v^2/2\omega_0}$. The adimensional decay rate γ is the ratio of photon to carrier lifetime $\gamma = \tau_{ph}/\tau_r$, while $\theta = (\omega_c - \omega_0)\tau_{ph}$ is the cavity detuning parameter, where ω_c is the longitudinal cavity frequency closest to ω_0 .

The bistability parameter Σ is defined as

$$\Sigma = \frac{L_A\omega_0}{n_b c T}; \quad (4)$$

Σ plays essentially the same role as the parameter C of optical bistability [30,31], used e.g. in the two-level saturable absorber model [11,32].

The 1D transverse Laplacian in the field equation (1) describes diffraction in the paraxial approximation, while in the carrier equation (2) represents carrier diffusion, with an adimensional diffusion coefficient d .

The radiation-matter interaction is described by the complex nonlinear susceptibility χ_{nl} , which is a function of the carrier density N and of the frequency of the injected field ω_0 . It is derived in the framework of the Semiconductor Bloch Equations theory [33]. In considering a MQW structure, we take into account the two main many-body effects which affect the optical response of the medium. The first one is the density-dependent contribution to the transition energy (the so-called band-gap renormalization), the second one is the Coulomb enhancement, calculated in the Padé approximation.

We will omit here the description of the explicit dependence of the nonlinear susceptibility χ_{nl} on the carrier density N and on the input frequency ω_0 : the reader can find it in a previous paper of ours [34].

We note that the mean field limit, that suppresses the longitudinal variations of the dynamical variables, is not a good approximation in this device, because of the length of the cavity (1 mm approximately) and of the poor reflectivity of one of the two mirrors of the cavity. Models that go beyond the mean field limit are under study [35], and will be the object of a future publication.

It is important to remark that thermal effects have not been included here, while they have been analyzed and modelled in a number of papers of ours [27,36,37]. Nevertheless, the model presented in this manuscript gives useful insights on the stationary spatial solutions of our uni-dimensional device, that is, on pattern and CS formation, while it cannot adequately describe the temporal behavior of these solutions.

In order to compare our predictions with the experiments, we have to take into account the relation between the intracavity field and the reflected field. In our notation, this relation for a Fabry-Perot resonator reads [38]:

$$\tilde{E}_R = \tilde{E}_I - \sigma \tilde{E}, \quad (5)$$

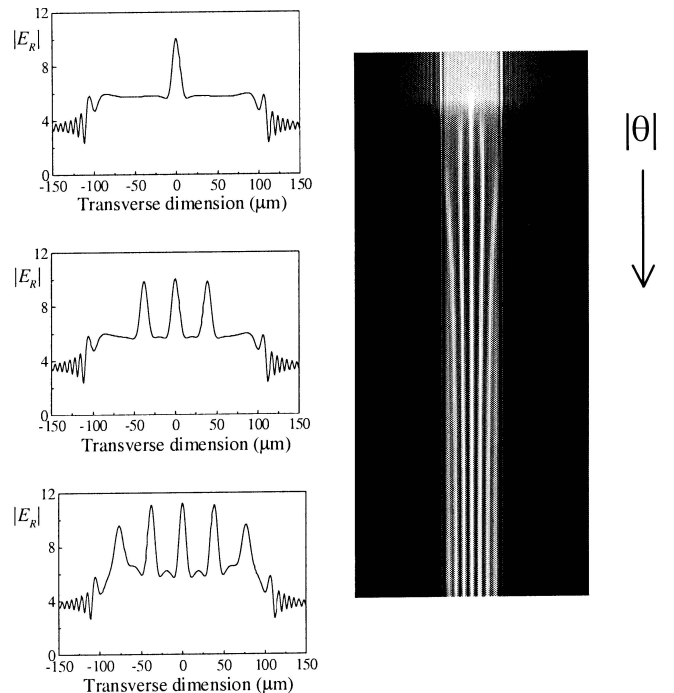


Fig. 8. Numerical transverse profile of the reflected field of the driven diode laser. As the input frequency is increased (the cavity detuning θ is decreased, becoming more negative), the number of peaks increases. The number of peaks is also visible from the gray-scale intensity diagram on the right.

where the parameter σ depends on the transmissivity of the front mirror: $\sigma = T_F/T$. Note that if the two mirrors have the same transmissivity $\sigma = 1$.

Following the usual procedure [28,29] we found the homogeneous steady states, and studied their stability against spatially modulated perturbations, by performing the linear stability analysis. In this way, we were able to find extended parametric ranges where a modulational instability of the Turing type affects the upper branch of the steady-state curve, while the lower branch is stable. This the most favorable scenario for finding cavity solitons.

We integrated numerically the dynamical equations, by means of a split-step code, assuming a top-hat profile for the current to simulate the finite extension of the gain region. This assumption is fundamental for the agreement between theory and experiments.

It is not possible to know the exact parametric values for a specific experimental measurement and therefore to match such values for experiment and theory. However, we can compare the trend as a specific parameter is changed. In Figure 8 we show the amplitude profile of the reflected field obtained by varying the frequency ω_0 of the driving field (the detuning parameter θ in the numerical plots). As ω_0 is increased (θ decreased) the number of peaks in the transverse profile increases. We can note the excellent agreement between theory and experiments, comparing with Figure 5.

The passage from a one-peaked structure to three-peaked, five-peaked and so on, which is also very well visible in the rightmost plot of Figure 8, is reminiscent

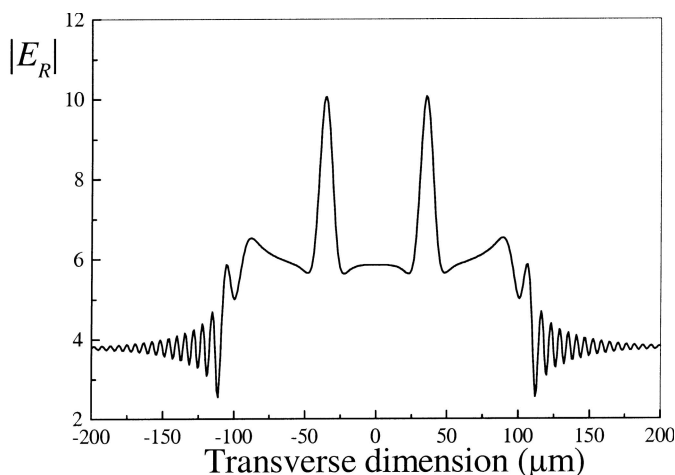


Fig. 9. Numerical transverse profile with two independent CSs present in the reflected field of the driven diode laser. These structures can be independently switched on and off.

of the sequence of bifurcations predicted in the general theory of reference [39]. However, our numerical simulations show that the structures shown in Figure 8 correspond to a truncated version of the full 1D pattern of the kind first predicted in reference [20], where the truncation is introduced by the finite size of the active region. The multi-peaked structures predicted in [39] correspond, instead, to localised boundary-independent structures with 3, 5... peaks.

Similar sequences can be obtained by varying the holding-beam intensity.

In Figure 9 we show a numerical reflected field profile where two CS are simultaneously present. These structures result totally independent of each other: they can be excited independently by means of localized laser pulses added to the holding-beam and they can be independently erased.

As for the thermal oscillations of one of the peaks in Figure 6, we have to mention that we did not find neither theoretically nor numerically any oscillation involving one single structure. In reference [27,37,36] we introduced a model including the lattice temperature dynamics, but we found regenerative oscillations of the whole beam [27,37] or a thermally induced motion of CS and patterns [36,37].

4 Conclusions

In summary, we have experimentally analyzed the spatio-temporal dynamics of the transverse structures appearing in broad area edge-emitting semiconductor amplifiers under CW optical injection. We have demonstrated that, in certain parameter ranges, the emission of the system exhibits a multi-peaked structure. The evolution of the structures with the parameters is compatible with an interpretation in terms of cavity solitons, but the tests performed reveal that these structures are strongly influenced by the transverse boundary conditions and they also seem influenced (pinning, addressing) by accidental defects in the

semiconductor medium. However, we have obtained two single-peak structures in the same device that exhibit uncorrelated dynamics. Therefore devices with larger Fresnel numbers are required in order to achieve the formation of *bona fide* CSs.

Finally, it must be noted that often self pulsation of the structures with periods on the order of 1 ms is observed, which can be explained in terms of regenerative thermal oscillations. The present indications are encouraging because they clearly show the basics of pattern formation and localisations of spatial structures; they open the path to new experiments employing lasers with larger Fresnel number and better transverse homogeneity, both material (s.c. medium) and electric (current profile). An improved heat sinking might provide the necessary taming of the thermal drifts affecting the stability of these structures. A similar route led to the observation of CS in semiconductor microresonators [23], after thermal and boundary effects were dealt with [22].

A model describing the dynamics of the system was introduced, taking into account the most relevant features of the real device, such as the 1D geometry and the finite current profile. By varying the input field frequency we were able to validate the phenomena observed experimentally: starting from a single-peak structure the reflected field displays three peaks and by increasing further the frequency a five-peaks pattern develops. Furthermore, by injecting an additional pulse (writing beam) into the sample, centered at two different positions, we were able to switch on and off two CSs independently.

This work was carried out in the framework of the ESPRIT LTR Project n. 28235 PIANOS, the PRIN project *Formazione e controllo di solitoni di cavità in microrisonatori a semiconduttore* of the Italian Ministry for University and Research, and the European Network VISTA (VCSELs for Information Society Technology Applications).

References

1. F.T. Arecchi, *Physica D* **51**, 450 (1991)
2. L.A. Lugiato, *Phys. Rep.* **219**, 293 (1992)
3. C.O. Weiss, *Phys. Rep.* **219**, 311 (1992)
4. L.A. Lugiato, *Chaos Solitons Fractals* **4**, 1251 (1994)
5. W.J. Firth, *Pattern formation in passive nonlinear optical systems*, in *Self-organization in optical systems and applications in information technology*, edited by M.A. Vorontsov, W.B. Miller (Springer-Verlag, 1995)
6. L.A. Lugiato, M. Brambilla, A. Gatti, *Optical Pattern Formation*, in *Advances in Atomic, Molecular and Optical Physics*, edited by B. Bederson, H. Walther (Academic Press, 1998), Vol. 40
7. J.V. Moloney, H.M. Gibbs, *Phys. Rev. Lett.* **48**, 1607 (1982)
8. D.W. Mc Laughlin, J.V. Moloney, A.C. Newell, *Phys. Rev. Lett.* **51**, 75 (1983)
9. N.N. Rosanov, G.V. Khodova, *Opt. Spectrosc.* **65**, 449 (1988)
10. M. Tlidi, P. Mandel, R. Lefever, *Phys. Rev. Lett.* **73**, 640 (1994)

11. W.J. Firth, A.J. Scroggie, Phys. Rev. Lett. **76**, 1623 (1996)
12. V.B. Taranenko, K. Staliunas, C.O. Weiss, Phys. Rev. A **56**, 1582 (1997)
13. K. Staliunas, V.J. Sanchez-Morcillo, Opt. Comm. **139**, 306 (1997)
14. C. Etrich, V. Peschel, F. Lederer, Phys. Rev. Lett. **79**, 2454 (1997)
15. V. Yu Bazhenov, V.B. Taranenko, M.V. Vasnetsov, Proc. Soc. Photo-Opt. Instrum. Eng. **1806**, 14 (1993)
16. M. Saffman, D. Montgomery, D.Z. Anderson, Opt. Lett. **19**, 518-520 (1994)
17. C.O. Weiss, M. Vaupel, K. Staliunas, G. Slekyš, V.B. Taranenko, Appl. Phys. B **68**, 151 (1999)
18. A. Schreiber, B. Thuring, M. Kreuzer, T. Tschudi, Opt. Commun. **136**, 415 (1997)
19. P.L. Ramazza, S. Ducci, S. Boccaletti, F.T. Arecchi, J. Opt. B: Quant. Semiclass. Opt. **2**, 399 (2000)
20. B. Schaebers, M. Feldmann, T. Ackemann, W. Lange, Phys. Rev. Lett. **85**, 748 (2000). This work provides clear-cut evidence of coexistence of pattern and homogeneous state
21. M. Brambilla, L.A. Lugiato, F. Prati, L. Spinelli, W.J. Firth, Phys. Rev. Lett. **79**, 2042 (1997); D. Michaelis, U. Peschel, F. Lederer, Phys. Rev. A **56**, R3366 (1997)
22. R. Kuszelewicz, I. Ganne, G. Slekyš, I. Sagnes, M. Brambilla, Phys. Rev. Lett. **84**, 6006 (2000); V.B. Taranenko, I. Ganne, R. Kuszelewicz, C.O. Weiss, Phys. Rev. A **61**, 063818 (2000); T. Ackemann et al., Opt. Lett. **25**, 814 (2000)
23. S. Barland, J.R. Tredicce, M. Brambilla, L.A. Lugiato, S. Balle, M. Giudici, T. Maggipinto, L. Spinelli, G. Tissoni, T. Knoedl, M. Miller, R. Jaeger, Nature **419**, 699 (2002)
24. L.A. Lugiato, R. Lefever, Phys. Rev. Lett. **58**, 2209 (1987)
25. S. Barland, O. Piro, M. Giudici, J. Tredicce, S. Balle, Phys. Rev. E **68**, 036209 (2003)
26. M. Tamburrini, L. Goldberg, D. Mehuys, Appl. Phys. Lett. **60**, 1292 (1992)
27. G. Tissoni et al., SPIE Proc. **4283**, 577 (2001); I. Perrini, G. Tissoni, M. Brambilla, T. Maggipinto, J. Opt. B: Quant. Semiclass. Opt. **6**, S369 (2004)
28. L. Spinelli, G. Tissoni, M. Brambilla, F. Prati, L.A. Lugiato, Phys. Rev. A **58**, 2542 (1998)
29. G. Tissoni, L. Spinelli, M. Brambilla, T. Maggipinto, I.M. Perrini, L.A. Lugiato, J. Opt. Soc. Am. B **16**, 2083 (1999); G. Tissoni, L. Spinelli, M. Brambilla, T. Maggipinto, I.M. Perrini, L.A. Lugiato, J. Opt. Soc. Am. B **16**, 2095 (1999)
30. R. Bonifacio, L.A. Lugiato, Lett. Nuovo Cim. **21**, 505 (1978)
31. H.M. Gibbs, *Optical Bistability: Controlling Light with Light* (Academic Press, New York, 1985)
32. M. Brambilla, L.A. Lugiato, M. Stefani, Europhys. Lett. **34**, 109 (1996); M. Brambilla, L.A. Lugiato, M. Stefani, Chaos **6**, 368 (1996)
33. W.W. Chow, S. Koch, M. Sargent III, *Semiconductor-Laser Physics* (Springer Verlag, Berlin, 1994)
34. L. Spinelli, G. Tissoni, M. Tarengi, M. Brambilla, Eur. Phys. J. D **15**, 257 (2001)
35. M. Brambilla, L. Columbo, T. Maggipinto, J. Opt. B: Quant. Semiclass. Opt. **6**, S197 (2004)
36. L. Spinelli, G. Tissoni, L. Lugiato, M. Brambilla, Phys. Rev. A **66**, 023817-12 (2002)
37. G. Tissoni, L. Spinelli, L.A. Lugiato, M. Brambilla, I. Perrini, T. Maggipinto, Opt. Expr. **10**, 1009 (2002)
38. M.J. Collett, C.W. Gardiner, Phys. Rev. A **30**, 1386 (1984)
39. C. Riera, P. Couillet, C. Tresser, Phys. Rev. Lett. **84**, 3069 (2000)